Sustainable Chemistry for Climate Action 2 (2023) 100015

Contents lists available at ScienceDirect

Sustainable Chemistry for Climate Action

journal homepage: www.elsevier.com/locate/scca

Fine tuning CO_2 adsorption and diffusion behaviors in ultra-microporous carbons for favorable CO_2 capture at moderate temperature

Ya-Qi Ba, Yong-Sheng Wang, Tian-Yi Li, Zhe Zheng, Guang-Ping Hao*, An-Hui Lu*

State Key Laboratory of Fine Chemicals, Liaoning Key Laboratory for Catalytic Conversion of Carbon Resources, School of Chemical Engineering, Dalian University of Technology, Dalian 116024, P. R. China

ARTICLE INFO

Keywords:
CO_2 capture
Adsorption kinetics
Microporous carbons
Carbon adsorbents

ABSTRACT

CO_2 capture from flue gas is one of the global urgent tasks. Adsorption separation of CO_2 is an energy-efficient way as compared to the absorption method. The central issue is to devise efficient adsorbents that work well under flue gas conditions with temperatures of 323–348 K and low CO_2 concentrations of 15%. In this work, we targeted this issue and proposed a well-controlled diffusion strategy, which is achieved over a series of poly(furfuryl alcohol)-derived carbons (PFCs) with dense and abundant ultra-micropores. As the adsorption temperature increased from 298 to 348 K, the CO_2 capture capacity is 54% kept for PFC-800, which is 1.2 times higher than that for samples without diffusion limitation. The capture of CO_2 is kinetics control at ambient temperature, however, at 348 K CO_2 with higher kinetic energy can overcome the restriction of the narrow pore entrance and the CO_2/N_2 selectivity for simulated flue gas composition increases from 20 to 40. Furthermore, the PFCs exhibit a high CO_2 volumetric adsorption capacity of 97 cm^3 cm^{-3} at 298 K and 1 bar, benefiting the practical application deployed with an integrated adsorption column. The diffusion kinetics can be further tuned when altering the bulk phase into nanocoating, which would inspire their application in different scenarios.

1. Introduction

The mitigation of CO_2 emissions remains one of the biggest challenges because of its negative effect on climate change [1–3]. Post-combustion capture from flue gas is one of the most promising solutions for reducing CO_2 emissions. It needs to capture CO_2 with a low concentration (*ca.* 15%) from a flue gas stream at a moderate temperature (323–348 K) [4]. Physisorption offers a promising alternative to the established energy-intensive processes in CO_2 capture because of its low energy consumption and mild operating conditions [5–7]. However, physisorption is a spontaneous exothermic process [8,9]. Thus, the development of advanced capture materials, especially porous adsorbents that can keep a good performance at moderate temperatures, is urgently needed [10,11]. Porous adsorbents including porous carbon [12–15], zeolites [16–18], and metal-organic frameworks (MOFs) [19,20], have been extensively studied for CO_2 capture. Among these adsorbents, porous carbons are regarded as one of the promising CO_2 adsorbents, due to their excellent chemical and thermal stability, tunable pore structure, relatively hydrophobic surface, low cost, and easy regeneration [21].

The design of porous carbon adsorbents is mainly based on thermodynamic and kinetic separation [22]. For thermodynamic separation, introducing basic sites into porous carbon, such as heteroatom doping and amine loading, could improve affinity for acidic CO_2 [23–26]. For instance, Lee et al. reported that using N-enriched polyacrylonitrile as a precursor could introduce N-containing functional groups into porous carbons. And a high CO_2 uptake of 3.03 mmol g^{-1} at 0 °C and 0.15 bar was achieved due to the enhanced interaction between the N sites and CO_2 [27]. Long et al. reported that mesoporous carbons decorated with polyethylenimine (PEI) showed an increase in sorption capacities as the temperature rose from 0 to 75 °C, which is 4.91 mmol g^{-1} at 75 °C and 1 bar [28]. However, its regeneration required a high energy consumption [1]. Alternatively, kinetic separation is another way that can be considered, which relies on different diffusion rates of adsorbates in the internal pores and allows for energy-efficient recovery [22]. An especially appealing approach is to control the diffusion rates of adsorbates with different molecular sizes by the alternation of the ultra-micropores (<0.7 nm) [29]. However, for porous carbons with complex slit-type ultra-micropores, the challenge is their markedly increased gas diffusion limitations [30], resulting in a longer equilibrium time and lower adsorption capacity. When the temperature rises to a moderate temperature e.g., 348 K as the case for flue gas sources, the diffusion limitation may be overcome due to the more intense molecular movements. Therefore, utilizing increased temperature to overcome diffusion limitations to compensate for adsorption capacity is a possible way to maintain the capture performance at moderate temperatures. Nevertheless, research

* Corresponding authors.
E-mail addresses: guangpinghao@dlut.edu.cn (G.-P. Hao), anhuilu@dlut.edu.cn (A.-H. Lu).

https://doi.org/10.1016/j.scca.2023.100015
Received 26 November 2022; Received in revised form 27 December 2022; Accepted 10 January 2023

on the influence of temperature and diffusion limitation on adsorption separation ability has rarely been reported.

Inspired by the above concept, we devised a series of poly(furfuryl alcohol) based ultra-microporous carbons (PFCs), which showed delicate suppression for CO_2 diffusion at ambient conditions but largely amended at increased temperatures e.g., 348 K. On such a basis, we transformed the kinetic issues into an effective strategy for practical CO_2 capture scenarios. By the rational construction of ultra-micropore, the PFCs with the appropriate diffusion limitation exhibit the highest adsorption capacity, which is up to the value of 96 cm^3 cm^{-3} at 298 K, and the capacity can keep 54% at 348 K. In particular, the adsorption capacity maintenance at 348 K is 1.2 times higher than that for the sample without diffusion limitation. Besides, PFCs show a high skeletal density of up to 1.96 g cm^3, which is conducive to achieving a high volumetric loading in the adsorption column. In addition, the poly(furfuryl alcohol) precursor can be nanocoated on various supports to serve as gas selective layers, which has the potential to be used in different separation scenarios.

2. Experimental

2.1. Materials

Furfuryl alcohol (FA, $C_5H_6O_2$, 98%), N, N-Dimethylformamide (DMF, C_3H_7NO, 98%) were purchased from Aladdin Chemistry Co., Ltd. (Shanghai, China). Oxalic acid (OA, $C_2H_2O_4$, 98%) was procured from Acros Organics (Geel, Belgium). Gas (N_2 99.999%, CO_2 99.995%, Ar 99.99%) were bought from Dalian Special gases Co., Ltd. (Dalian, China).

2.2. Synthesis of PFCs

A certain amount of FA, e.g., 4 mL, used as polymer monomer, and 90.4 mg of OA as polymerization catalyst were mixed and dissolved in a glass reactor at room temperature. The sealed reactor was transferred into an oven and cured at 50 °C for 24 h, then the temperature was increased to 90 °C and maintained for another 24 h. Next, the polymer was dried at 90 °C in air for 24 h. Afterward, the polymer was treated at 150 °C for 3 h, then heated to 300 °C with a heating rate of 1 °C min^{-1}. Followingly, the temperature increased to 400, 600, 800, and 1000 °C with a heating rate of 5 °C min^{-1} and maintained at that temperature for 2 h. The obtained PFCs were denoted as PFC-400, PFC-600, PFC-800, and PFC-1000, respectively.

2.3. Synthesis of C@HC

Honeycomb cordierite (HC) was used without any treatment. FA solution was polymerized by the above method for 24 h to obtain PFA. Dissolve 10 mL of PFA in 10 mL of DMF to produce the p-PFA solution. PFA@HC was obtained after dipping the HC in p-PFA solution at 25 °C for 30 min and then polymerized in air at 90 °C for 17 h. The obtained PFA@HC was placed into a porcelain boat and treated following the above procedure described to obtain the nanocoated C@HC.

2.4. Characterization

A TriStar 3000 physical adsorption analyzer (Micromeritics) was used to measure N_2 adsorption-desorption isotherms at 77 K. CO_2 adsorption-desorption isotherms were measured using an Autosorb-iQMP automated gas sorption analyzer (Quantachrome). Micropore size distributions (PSDs) were calculated by applying the Non-Local Density Functional Theory (NLDFT) to the CO_2 adsorption isotherms. A vapor sorption volumetric gas sorption analyzer (Vstar Quantachrome) was applied to collect water vapor adsorption-desorption isotherms. Before each adsorption experiment, the sample was degassed at 200 °C overnight. X-ray diffraction (XRD) measurement was on an X-ray diffractometer (Panalytical X'pert) with a monochromatic Cu Kα (λ=1.54 Å) radiation source at 40 kV, 40 mA. Transmission electron microscopy (TEM) images were obtained with a Tecnai G220S-Twin instrument (FEI) operating at 200 kV. FTIR (Nicolet 6700) was used for elemental analysis and speculation on chemical bonding information. Field-emission scanning electron micrographs (SEM) images were obtained with a UHR FE-SEM SU8200 instrument (Hitachi).

2.5. Gas adsorption kinetic measurements

The time-dependent adsorption profiles of CO_2 and N_2 were collected on an IGA-100 Intelligent Gravimetric Analyzer (Hiden Analytical). The adsorbents were activated at 200 °C overnight under vacuum. The adsorption kinetic curves were carried out at 167 or 833 mbar for CO_2 and N_2, respectively. Here, based on the assumption that the adsorbent particles are spherical, we refer to the slopes in the initial region for the evaluation of diffusion time constants (D/r^2) *via* Fick's second law [31]

$$\frac{M_t}{M_\infty} = \frac{6}{\sqrt{\pi}} \cdot \sqrt{\frac{Dt}{r^2}} \left(\frac{M_t}{M_\infty} < 0.3\right) \quad (1)$$

where, M_t is the gas uptake at time t, M_∞ is the gas uptake at equilibrium, D is the diffusivity and r is the radius of the equivalent spherical particle.

2.6. Dynamic gas separation experiment

Dynamic gas-separation experiments were conducted using a stainless-steel column with an inner diameter of 8.0 mm and a packed length of 120 mm. The adsorbent of 40–60 mesh was packed into the column operated at temperatures in the range 298–348 K and pressure of 1 bar. The adsorbent column was firstly purged by Ar with a flow rate of 50 mL min^{-1} for 2 h at the target temperature. The gas mixture (CO_2/N_2, 16.7/83.3 v/v) was then introduced at 3 mL min^{-1}. Outlet gas from the column was monitored using a GC 9890T gas chromatograph (Techcomp) with a thermal conductivity detector (TCD). The blank experiment was also conducted under identical conditions but with a column filled with quartz sand to determine the volume of dead space. The (absolute) adsorbed amount is calculated from the breakthrough curve by the following Eq. (2):

$$q_i = \frac{F_0 \times t_0 - V_{dead} - \int_0^{t_0} F_i \Delta t}{m} \quad (2)$$

where, F_0 is the total volumetric gas flow rate; t_0 is the adsorption time (min); V_{dead} is the dead space of the column and line; F_i is the effluent volumetric flow rate; m is the mass of adsorbent.

3. Results and discussion

3.1. Pore structure analysis

The N_2 adsorption technique was employed to determine the porous structures for those samples [32]. The PFCs adsorbents pyrolyzed at 600, 800, and 1000 °C showed essentially zero N_2 uptakes, indicating the pores of PFCs were inaccessible to N_2 molecules at 77 K (Fig. S1) [33]. Therefore, we employed CO_2 as the gas probe to determine the micropore structure at 273 K because of its smaller kinetic diameter as compared to N_2 (Fig. 1a) [34]. The high CO_2 uptakes denote abundant micropore porosity for PFCs (Table S1). Due to the absence of macropores and mesopores, the PFCs display a high skeletal density of up to 1.96 g cm^{-3} (Fig. S2), which is advantageous for achieving a high volumetric uptake [18]. As the pyrolysis temperature increased from 600 to 800 °C, the CO_2 volumetric adsorption capacity increased from 70 to 115 cm^3 cm^{-3}, which result from the formation of new micropores through further thermal decomposition of the carbonaceous matter

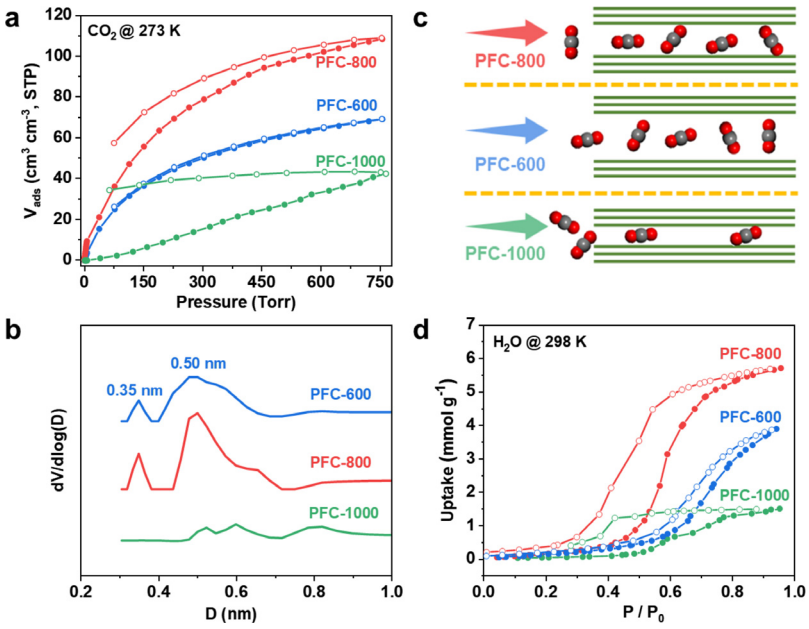

Fig. 1. (a) CO_2 adsorption-desorption isotherms at 273 K. (b) The PSDs for PFCs by CO_2 adsorption at 273 K. (c) Schematic of CO_2 diffusion in the narrow pores of PFCs. (d) Water vapor adsorption-desorption isotherms at 298 K.

[35]. Besides, the gravimetric CO_2 adsorption capacity is shown in Fig. S3. As the pyrolysis temperature increased further to 1000 °C, the CO_2 adsorption capacity reduced to 42 cm^3 cm^{-3} due to pore shrinkage and collapse [35]. Notably, the desorption branch of the isotherm did not follow adsorption at lower pressures (P/P_0 <0.003), i.e., low-pressure hysteresis. The PFCs showed an enhanced low-pressure hysteresis as the pyrolysis temperature increased. For PFC-800 with a large pore volume of 0.162 cm^3 g^{-1}, the low-pressure hysteresis can still be observed clearly. Particularly, PFC-1000 showed striking irreversibility in CO_2 adsorption, and almost 34 cm^3 cm^{-3} CO_2 could not be desorbed when P/P_0 <0.003. This can be predicted from the CO_2 adsorption isotherm for PFC-1000 at 273 K, which shows that the uptake increased linearly with increasing adsorption pressure without any micropore filling phenomenon. This indicates that either there is a lack of micropores or the pore size is too narrow to allow CO_2 to get into. For the same reason, it requires very low pressure (P/P_0 <0.003) for its desorption.

When the carbonization temperature is 400 °C, the ultramicroporous structure has been generated with an ultra-micropore volume of 0.06 cm^3 g^{-1} (Fig. S4). As the pyrolysis temperature increased to 800 °C, the ultra-micropore volume increased to the maximum of 0.13 cm^3 cm^{-3}. A bimodal PSD centered at 0.35 and 0.50 nm was obtained for PFC-600 and PFC-800 based on the NLDFT from CO_2 adsorption isotherms (Fig. 1b). However, as the temperature increased to 1000 °C, the peak pore size that is at 0.35 nm disappeared, but that centered at 0.80 nm became evident. As presumed by the low-pressure hysteresis, there are ultra-micropores narrower than 0.35 nm in the PFC-1000, but could not be detected due to test accuracy. The XRD patterns (Fig. S5) were obtained to analyze the carbonaceous structure of PFCs. The peaks at 22.3 and 43.1° are characteristic of (002) and (100) crystal planes of graphitic carbon [36]. These two peaks of PFCs sharpened gradually with increasing pyrolysis temperature, indicating an increase in the graphitization degree. TEM images show that when the carbonization temperature increases, it becomes locally graphitic at the edge part (Fig. S6). In addition, the variation of the graphitic structure was characterized by FT-IR spectra (Fig. S7). The peak located at around 1622 cm^{-1} (corresponding to aromatic ring conjugated C=C groups) in PFC-600 was shifted to lower 1601 cm^{-1} (corresponding to aromatic C=C groups) in PFC-800 and PFC-1000, indicating the growth of graphene lattices [37]. The schematic of CO_2 diffusion in the pores of PFCs was further proposed (Fig. 1c). The PFC-600 shows dominant wormlike micropores. The average pore size is around 0.50 nm, which ensures the free diffusion of guest CO_2. Increasing the carbonization temperature led to the shrinkage of the micropores. For instance, the micropore size is estimated to be 0.48 nm. Thus, the diffusion of CO_2 is suppressed. For PFC-1000, perhaps only at a specific angle can CO_2 diffuse into pores, so that it exhibits striking irreversibility in CO_2 adsorption.

Water molecules with a small kinetic diameter of 0.27 nm and strong dipole can sensitively reflect the pore structure and surface chemistry of porous materials [38]. Therefore, water vapor adsorption-desorption isotherms were measured (Fig. 1d). The water vapor uptake of PFC-800 is up to 5.7 mmol g^{-1}, which is 1.5 and 3.8 times higher than that of PFC-600 and PFC-1000. The changing trend of water vapor uptake

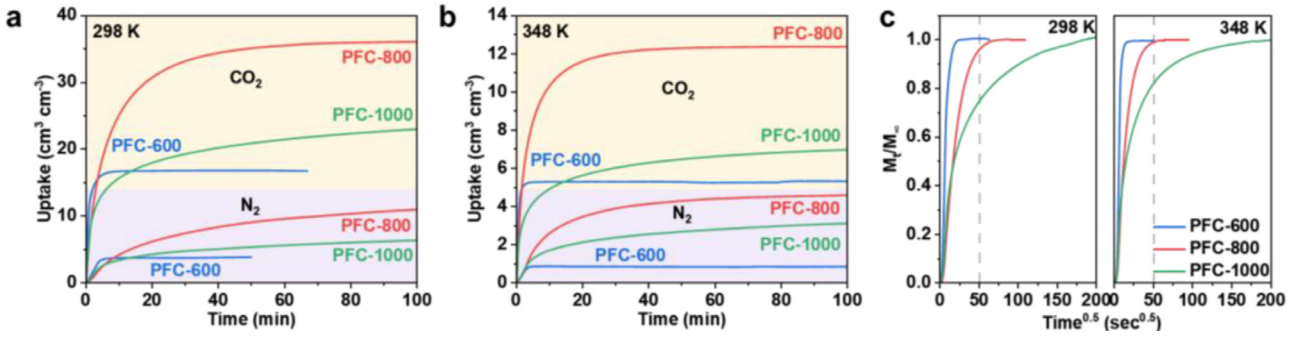

Fig. 2. Transient adsorption curve for CO_2 and N_2 at (a) 298 K and (b) 348 K on PFCs. (c) Adsorption kinetics profiles for CO_2 at 298 K and 348 K on PFCs.

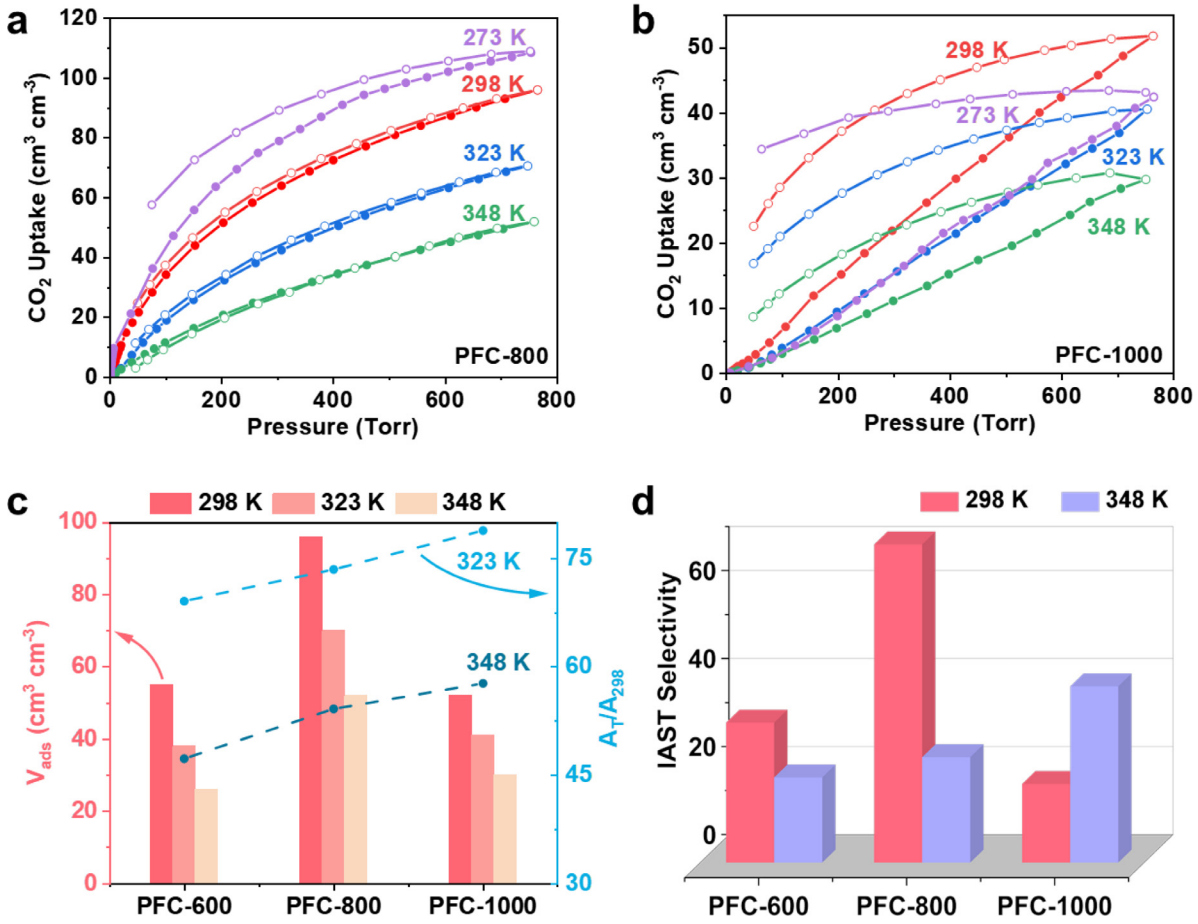

Fig. 3. CO_2 adsorption-desorption isotherms for (a) PFC-800 and (b) PFC-1000 at 273, 298, 323, and 348 K. (c) Static adsorption capacity and maintenance ratio of PFCs at 298, 323, and 348 K. (d) IAST selectivity for CO_2/N_2 (16.7/83.3 v/v) at 1 bar and different temperatures (298 and 348 K).

is similar to that of CO_2 uptake, denoting the similar forces and pore utilization on water vapor and CO_2 adsorption. The PFCs display low uptakes at low pressure of $P/P_0 < 0.3$, reflecting the weak polarity. This demonstrates that the adsorption uptake differences stem from the differences of ultra-micropore rather than surface functional group interactions [28]. Interestingly, the slope of desorption isotherm decreases gradually as the pyrolysis temperature increases when $P/P_0 > 0.5$, proving a decreasing diffusion limitation.

3.2. Adsorption kinetics of CO_2 and N_2 on PFCs

To explore the gas diffusion behavior of the CO_2/N_2 in the ultra-micropore of PFCs, the time-resolved gas adsorption for CO_2 and N_2 was measured (Fig. 2a and b). As we previously assumed, the diffusion rates on PFCs for CO_2 and N_2 are reduced incrementally as pyrolysis temperature increases, owing to the pore shrinkage. Moreover, the diffusion and uptake differences between CO_2 and N_2 are clear. In particular, PFC-800 exhibits a CO_2 uptake of 36 cm^3 cm^{-3} at 298 K and 167 mbar, while the N_2 uptake is 13 cm^3 cm^{-3} at 298 K and 833 mbar, indicating the separation ability of PFCs. For PFC-800, CO_2 reached the equilibrium within 40 min at 298 K, including 10 min of rapid diffusion to reach more than 70% of the saturation adsorption capacity. However, N_2 did not reach equilibrium until 100 min at 298 K, displaying the strong suppression for N_2 diffusion. As the operating temperature rose to 348 K, the diffusion rate for both CO_2 and N_2 increased. The CO_2 adsorption capacity of PFC-800 reached more than 90% of the saturation adsorption capacity of 12 cm^3 cm^{-3} within 10 min at 348 K. Nevertheless, the N_2 uptake was still increasing slowly at 100 min, but with a smaller slope than that at 298 K. Interestingly, PFC-1000 exhibits a higher adsorption capacity than PFC-600 when the equilibrium time is long enough, which is in contrast to the static adsorption results. Especially, the CO_2 uptake of 23 cm^3 cm^{-3} for PFC-1000 at 100 min is 1.4 times higher than PFC-600. This reflected the presence of ultra-microporous volumes of PFC-1000 that cannot be detected by static adsorption with insufficient equilibrium time due to the slow diffusion rate, as we speculated in the previous section.

To further quantify the effect of operating temperature on diffusion, the diffusional time constants ($D' = D/r^2$) for CO_2 and N_2 were calculated respectively (Figs. 2c and S8, Table S2) [31,39]. The CO_2 diffusional time constant for PFC-800 at 348 K is 2.86×10^{-11}, which is 2.9 times higher than that of 9.68×10^{-12} at 298 K. However, the ratio of the diffusion time constant at 348 K to that at 298 K is 1.4 and 2.1 for PFC-600 and PFC-1000, respectively. This reflects the highest compensation of CO_2 diffusion by raising temperature requires appropriate diffusion limitations. In addition, the kinetic selectivity ($D'(CO_2)/D'(N_2)$) was calculated to be 6.0 for PFC-1000 at 348 K, which is 1.7 times higher than that of 3.6 at 298 K, indicating that increasing temperature compensates more for CO_2 diffusion than N_2 diffusion.

3.3. CO_2 capture performance of PFCs at moderate temperatures

To investigate the effect of operating temperature on the CO_2 capture performance of carbon materials with different diffusion limitations, the CO_2 and N_2 adsorption-desorption isotherms of PFCs at different temperatures are measured (Figs. 3a and b and S9). There is a gradual decrease in the CO_2 adsorption capacity for PFC-600 and PFC-800 as the operating temperature increases from 273 K to 348 K. It is worth noting that the CO_2 adsorption capacity of PFC-1000 at 273 K was 9 cm^3 cm^{-3}

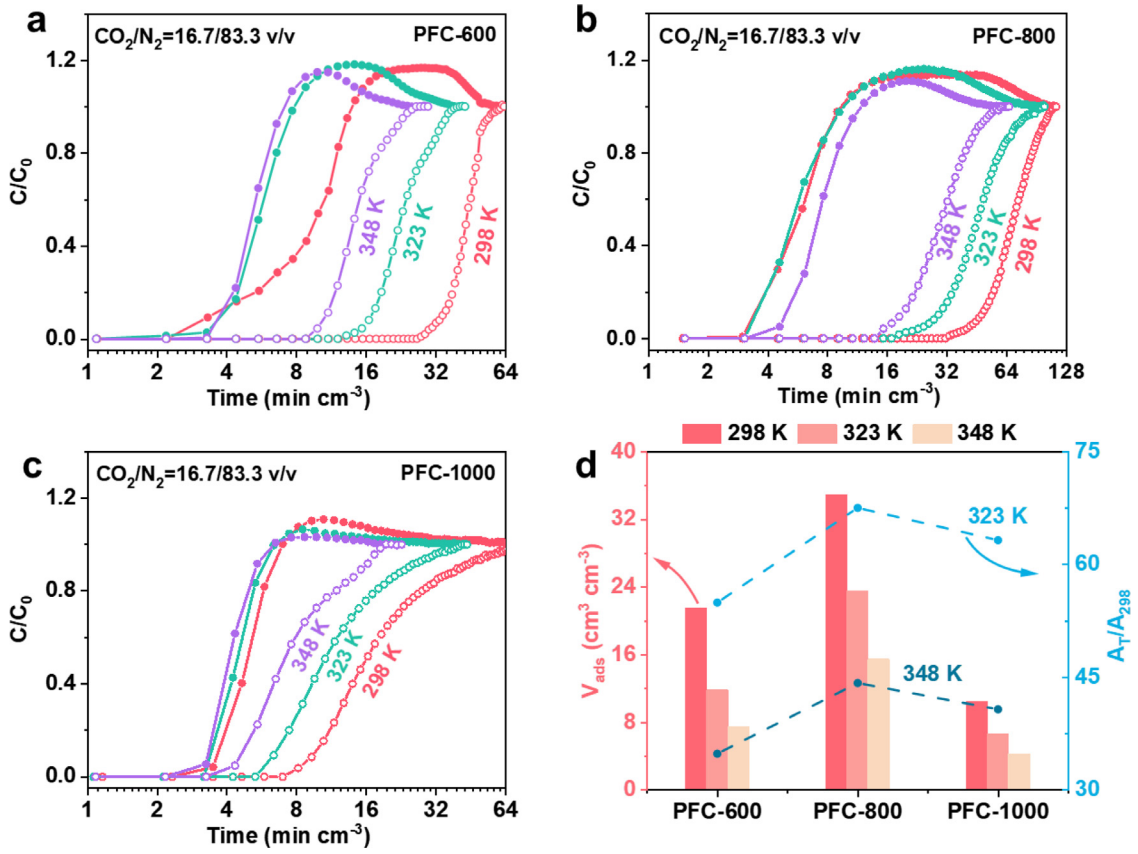

Fig. 4. Breakthrough curves of PFCs pyrolysis at (a) 600, (b) 800, and (c)1000 °C for CO_2/N_2 (16.7/83.3 v/v) mixture with a flow rate of 3 mL min^{-1} at temperatures in the range 298–348 K and pressures of 1 bar. (d) Dynamic adsorption capacity and maintenance ratio of PFCs at 298, 323, and 348 K.

lower than that at 298 K, and 2 cm^3 cm^{-3} higher than that at 323 K (Fig. 3b). This further confirms that the CO_2 kinetic energy imparted by an appropriate temperature increase can compensate for the adsorption capacity with CO_2 diffusion limitation. However, the CO_2 adsorption isotherms of PFC-1000 at 323 K are similar to that at 273 K, indicating that diffusion limitation is not the dominant factor influencing the adsorption capacity anymore. The increased CO_2 molecular kinetic energy as the temperature rrises will reduce the adsorption capacity. The calculation results of the ratio of the adsorption capacity at 323 or 348 K to that at 298 K, i.e., the adsorption capacity maintenance ratio at 323 or 348 K show a steady increase for PFCs as diffusion limitation increases (Fig. 3c). The CO_2 adsorption capacity maintenance ratio for PFC-1000 at 323 K and 348 K are up to 79% and 58%, which is 15% and 24% increase compared to PFC-600, respectively. In addition, the CO_2 capacity maintenance ratio at 323 K of PFCs is higher than those of many other reported porous carbons (Table S3).

The ideal selectivity of CO_2/N_2 mixtures (16.7/83.3 v/v) was further calculated based on the ideal adsorbed solution theory (IAST, Fig. 3d and S10) [26]. The highest IAST selectivity among the PFCs at 298 K and 1 bar is 72 for PFC-800, while that at 348 K and 1 bar is 40 for PFC-1000. Furthermore, the low-pressure hysteresis in the CO_2 adsorption-desorption isotherm at 348 K of PFC-1000 is still obvious, while the desorption branch of the isotherm followed adsorption for PFC-800 at 348 K. PFC-800 with the highest CO_2 uptake and appropriate diffusion limitation is deemed to be a more optimal adsorbent due to the negative effects of excessive diffusion limitations on practical applications.

3.4. Breakthrough experiments for CO_2/N_2 mixture on PFCs

To confirm the validity of the PFCs for practical separation performance, column breakthrough experiments were conducted that simulating a flue gas condition, namely in a mixture of CO_2/N_2 (16.7/83.3 v/v) at 298–348 K and 1 bar (Fig. 4a-c). N_2 immediately eluted from the adsorption column, and all the PFCs displayed the breakthrough time within 4 min cm^{-3}. Then CO_2 flowed through the column and the slope of the CO_2 breakthrough curve became smaller as the diffusion limitation of PFCs enhanced. Their adsorption capacity under breakthrough conditions was calculated (Fig. 4d). Similar to static adsorption, PFC-800 exhibits the highest adsorption capacity at all temperatures. The CO_2 did not elute out until 32 min on PFC-800 at 298 K, which is equivalent to a dynamic adsorption capacity of around 35 cm^3 cm^{-3}. For PFC-1000, the CO_2 uptake is 10 cm^3 cm^{-3} under identical conditions. Notably, unlike the static result, the highest dynamic adsorption capacity maintenance ratio at 323 and 348 K is 68% and 44% for PFC-800, which is 1.2 and 1.3 times higher than that of PFC-600, and both 1.1 times higher than that of PFC-1000, respectively. The negative impacts of excessive diffusion limitation for practical applications are demonstrated. In summary, PFC-800 with the best compromise between adsorption capacity and adsorption capacity maintenance ratio is the promising adsorbent for CO_2 capture from fuel gas.

3.5. PFCs nanocoating

In preparation of poly(furfuryl alcohol), we found the viscosity of the precursor is relatively high and sticky, which can be readily coated on various support materials such as honeycomb cordierite (HC). HC supports with large parallel channels show the evident advantage of low-pressure drop. Following the protocols as depicted in Fig. 5a, we prepared the supported PFCs nano-coating. SEM results showed that after coating, a C@HC with smooth and dense surface morphology had been formed (Fig. 5b). Due to the rough and porous structure of HC (Fig. S11a and b), the p-PFA solution not only covers its surface but

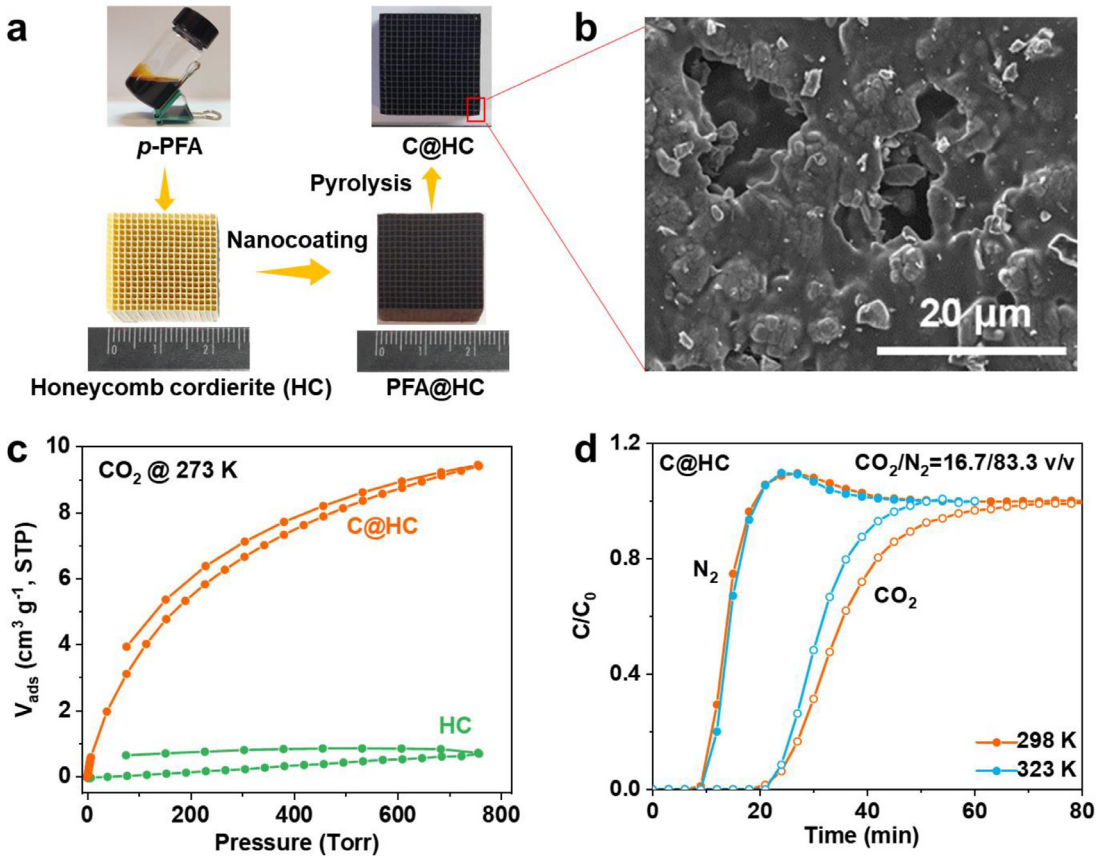

Fig. 5. (a) Schematic illustration for the preparation of C@HC. (b) SEM image of C@HC. (c) CO_2 adsorption-desorption isotherms at 273 K. (d) Breakthrough curves for CO_2/N_2 (16.7/83.3 v/v) mixture with a flow rate of 3 mL min^{-1} at 298 and 323 K.

also soaks into its interior to form a homogeneous coating. The honeycomb structure was maintained with an outer gas selective carbon layer of *ca.* 8 μm and a rough inner support surface (Fig. S11c and d). Compared to the adsorbents with a particle size of around 500 μm, the gas diffusion path reduces around 60 times, which is beneficial to the CO_2 adsorption kinetic. We further measured the CO_2 adsorption-desorption isotherms (Fig. 5c) and found that the CO_2 adsorption capacity for C@HC increased by 13.5 times compared to the HC, and CO_2 can be desorbed easily. Furthermore, the breakthrough experiment for CO_2/N_2 (16.7/83.3 v/v) mixture also shows that the separation time of C@HC is 11 min longer than that of HC (Fig. S12), indicating the effective coating of PFC with CO_2 separation properties on HC. Excitingly, the C@HC shows the same CO_2/N_2 separation performance at 323 K compared with that at 298 K. And shorter equilibrium times reflected larger CO_2 molecular kinetic energy to overcome the diffusion limitation. In addition, for C@HC, CO_2 eluted from the adsorption column with a sharper slope than that for the PFC monolith due to the reduction of the diffusion path. We assume that modulating the coating thickness could achieve better CO_2 capture in fuel gas conditions. The follow-up work is underway.

4. Conclusions

In summary, we reported an effective strategy to enhance the separation performance at moderate temperatures over a series of poly(furfuryl alcohol) based ultra-microporous carbons. Utilizing the kinetic energy provided by increased temperatures, the CO_2 diffusion limitation is overcome to offset the loss of the CO_2 uptake that normally as increasing the adsorption temperature. This concept has been demonstrated as an appealing strategy for CO_2 capture from fuel gas, which represents a fresh idea in designing targeted adsorbents. Furthermore, the poly(furfuryl alcohol) precursor can be nanocoated on various supports to function as gas selective layers, which can be employed in a variety of separation applications.

Declaration of Competing Interest

The authors declare that they have no known competing financial interests or personal relationships that could have appeared to influence the work reported in this paper.

CRediT authorship contribution statement

Ya-Qi Ba: Conceptualization, Data curation, Investigation, Methodology, Validation, Writing – review & editing. **Yong-Sheng Wang:** Conceptualization, Methodology, Writing – review & editing. **Tian-Yi Li:** Writing – review & editing. **Zhe Zheng:** Validation. **Guang-Ping Hao:** Conceptualization, Methodology, Validation, Supervision, Project administration, Funding acquisition, Writing – review & editing. **An-Hui Lu:** Supervision, Funding acquisition, Writing – review & editing.

Data availability

Data will be made available on request.

Acknowledgments

This work was supported by the National Natural Science Foundation of China (grant numbers 22275027, 21975037); the Fundamental Research Funds for the Central Universities (grant numbers DUT22QN206, DUT20GJ215).

Supplementary materials

Supplementary material associated with this article can be found, in the online version, at doi:10.1016/j.scca.2023.100015.

References

[1] R.S. Siegelman, E.J. Kim, J.R. Long, Porous materials for carbon dioxide separations, Nat. Mater. 20 (2021) 1060–1072, doi:10.1038/s41563-021-01054-8.

[2] M. Bui, C.S. Adjiman, A. Bardow, E.J. Anthony, A. Boston, S. Brown, P.S. Fennell, S. Fuss, A. Galindo, L.A. Hackett, J.P. Hallett, H.J. Herzog, G. Jackson, J. Kemper, S. Krevor, G.C. Maitland, M. Matuszewski, I.S. Metcalfe, C. Petit, G. Puxty, J. Reimer, D.M. Reiner, E.S. Rubin, S.A. Scott, N. Shah, B. Smit, J.P. Martin Trusler, P. Webley, J. Wilcox, N.M. Dowell, Carbon Capture and Storage (CCS): the Way Forward, Energy Environ. Sci. 11 (5) (2018) 1062–1176, doi:10.1039/C7EE02342A.

[3] J. Hu, P. Hongmanorom, J. Chen, W. Wei, P. Chirawatkul, V.V. Galvita, S. Kawi, Tandem distributing ni into Cao framework for isothermal integration of CO_2 capture and conversion, Chem. Eng. J. 452 (2023) 139460, doi:10.1016/j.cej.2022.139460.

[4] R.S. Liu, X.D. Shi, C.T. Wang, Y.Z. Gao, S. Xu, G.P. Hao, A.H. Lu, Advances in post-combustion CO_2 capture by physical adsorption: from materials innovation to separation practice, ChemSusChem 14 (6) (2021) 1428–1471, doi:10.1002/cssc.202002677.

[5] L.P. Guo, W.C. Li, B. Qiu, Z.X. Ren, J. Du, A.H. Lu, Interfacial assembled preparation of porous carbon composites for selective CO_2 capture at elevated temperatures, J. Mater. Chem. A 7 (2019) 5402–5408, doi:10.1039/C8TA12122B.

[6] M. Oschatz, M. Antonietti, A search for selectivity to enable CO_2 capture with porous adsorbents, Energy Environ. Sci. 11 (2018) 57–70, doi:10.1039/C7EE02110K.

[7] G. Singh, J. Lee, A. Karakoti, R. Bahadur, J. Yi, D. Zhao, K. AlBahilyc, A. Vinu, Emerging trends in porous materials for CO_2 capture and conversion, Chem. Soc. Rev. 49 (2020) 4360–4404, doi:10.1039/D0CS00075B.

[8] X. Shi, H. Xiao, H. Azarabadi, J. Song, X.-.L. Wu, X. Chen, K.S. Lackner, Sorbents for the Direct Capture of CO_2 from Ambient Air, Angew. Chem. Int. Ed. 59 (2019) 6984–7006, doi:10.1002/anie.201906756.

[9] J. Du, W.C. Li, Z.X. Ren, L.P. Guo, A.H. Lu, Synthesis of mechanically robust porous carbon monoliths for CO_2 adsorption and separation, J. Energy Chem. 42 (2019) 56–61, doi:10.1016/j.jechem.2019.06.006.

[10] D.W. Keith, G. Holmes, D.S. Angelo, K. Heidel, A process for capturing CO_2 from the atmosphere, Joule 2 (2018) 1573–1594, doi:10.1016/j.joule.2018.05.006.

[11] D.M. D'Alessandro, B. Smit, J.R. Long, Carbon dioxide capture: prospects for new materials, Angew. Chem. Int. Ed. 49 (2010) 6058–6062, doi:10.1002/anie.201000431.

[12] J.A. Cecilia, E. Vilarrasa-García, N. Chouikhi, R. Morales-Ospino, S. Besghaier, M. Chlendi, M. Bagane, M. Bastos-Neto, D.C.S. Azevedo, E. Rodríguez-Castellóna, Activated carbons synthesized from sucrose using porous clay heterostructures as template for CO_2 adsorption, Sustain. Chem. Climate Action 1 (2022) 100006, doi:10.1016/j.scca.2022.100006.

[13] A. Altwala, R. Mokaya, Rational synthesis of microporous carbons for enhanced post-combustion CO_2 capture *via* non-hydroxide activation of air carbonised biomass, RSC Adv. 12 (31) (2022) 20080–20087, doi:10.1039/D2RA02661A.

[14] L.P. Guo, Q.T. Hu, P. Zhang, W.C. Li, A.H. Lu, Polyacrylonitrile-derived sponge-like micro/macroporous carbon for selective CO_2 separation, Chem. Eur. J. 24 (33) (2018) 8369–8374, doi:10.1002/chem.201800631.

[15] S. Wang, Y. Li, S. Dai, D.E. Jiang, Prediction by convolutional neural networks of CO_2/N_2 selectivity in porous carbons from N_2 adsorption isotherm at 77K, Angew. Chem. Int. Ed. 59 (44) (2020) 19645–19648, doi:10.1002/anie.202005931.

[16] O. Cheung, Z. Bacsik, N. Fil, P. Krokidas, D. Wardecki, N. Hedin, Selective adsorption of CO_2 on zeolites Nak-ZK-4 with Si/Al of 1.8-2.8, ACS Omega 5 (39) (2020) 25371–25380, doi:10.1021/acsomega.0c03749.

[17] M. Sun, Q. Gu, A. Hanif, T. Wang, J. Shang, Transition metal cation-exchanged SSZ-13 zeolites for CO_2 capture and separation from N_2, Chem. Eng. J. 370 (2019) 1450–1458, doi:10.1016/j.cej.2019.03.234.

[18] Y. Zhou, J. Zhang, L. Wang, X. Cui, X. Liu, S.S. Wong, H. An, N. Yan, J. Xie, C. Yu, P. Zhang, Y. Du, S. Xi, L. Zheng, X. Cao, Y. Wu, Y. Wang, C. Wang, H. Wen, L. Chen, H. Xing, J. Wang, Self-assembled iron-containing mordenite monolith for carbon dioxide sieving, Science 373 (6552) (2021) 315–320, doi:10.1126/science.aax5776.

[19] Z. Li, P. Liu, C. Ou, X. Dong, Porous metal-organic frameworks for carbon dioxide adsorption and separation at low pressure, ACS Sustain. Chem. Eng. 8 (2020) 15378–15404, doi:10.1021/acssuschemeng.0c05155.

[20] J. Jiang, Z. Lu, M. Zhang, J. Duan, W. Zhang, Y. Pan, J. Bai, Higher symmetry multinuclear clusters of metal-organic frameworks for highly selective CO_2 capture, J. Am. Chem. Soc. 140 (51) (2018) 17825–17829, doi:10.1021/jacs.8b07589.

[21] Y.S. Wang, X.J. Zhang, Y.Q. Ba, T.Y. Li, G.P. Hao, A.H. Lu, Recent advances in carbon-based adsorbents for adsorptive separation of light hydrocarbons, Research 2022 (2022) 9780864, doi:10.34133/2022/9780864.

[22] Y.F. Yuan, Y.S. Wang, X.L. Zhang, W.C. Li, G.P. Hao, L. Han, A.H. Lu, Wiggling mesopores kinetically amplify the adsorptive separation of propylene/propane, Angew. Chem. Int. Ed. 60 (35) (2021) 19063–19067, doi:10.1002/anie.202106523.

[23] Z.Y. Sui, Y.N. Meng, P.W. Xiao, Z.Q. Zhao, Z.X. Wei, B.H. Han, Nitrogen-doped graphene aerogels as efficient supercapacitor electrodes and gas adsorbents, ACS Appl. Mater. Interfaces 7 (3) (2015) 1431–1438, doi:10.1021/am5042065.

[24] P. Zhang, Y. Zhong, J. Ding, J. Wang, M. Xu, Q. Deng, Z. Zeng, S. Deng, A new choice of polymer precursor for solvent-free method: preparation of N-enriched porous carbons for highly selective CO_2 capture, Chem. Eng. J. 355 (2019) 963–973, doi:10.1016/j.cej.2018.08.219.

[25] J. Wang, R. Krishna, T. Yang, S. Deng, Nitrogen-rich microporous carbons for highly selective separation of light hydrocarbons, J. Mater. Chem. A 4 (36) (2016) 13957–13966, doi:10.1039/C6TA04939G.

[26] G. Rother, U. Tumuluri, K. Huang, W.T. Heller, S. Dai, J.M. Carrillo, B.G. Sumpter, Interactions of an imine polymer with nanoporous silica and carbon in hybrid adsorbents for carbon capture, Langmuir 37 (15) (2021) 4622–4631, doi:10.1021/acs.langmuir.1c00305.

[27] Y.K. Kim, G.M. Kim, J.W. Lee, Highly porous N-doped carbons impregnated with sodium for efficient CO_2 capture, J. Mater. Chem. A 3 (20) (2015) 10919–10927, doi:10.1039/C5TA01776A.

[28] J. Wang, M. Wang, B.B. Zhao, W.M. Qiao, D.H. Long, L.C. Ling, Mesoporous carbon-supported solid amine sorbents for low-temperature carbon dioxide capture, Ind. Eng. Chem. Res. 52 (15) (2013) 5437–5444, doi:10.1021/ie303388h.

[29] L.S. Blankenship, R. Mokaya, Modulating the porosity of carbons for improved adsorption of hydrogen, carbon dioxide, and methane: a review, Mater. Adv. 3 (2022) 1905–1930, doi:10.1039/D1MA00911G.

[30] Y.S. Wang, T.Y. Li, Y.Q. Ba, Z. Zheng, G.P. Hao, A.H. Lu, Mortar-and-cobblestone" type carbon pellets with interlinked C_3H_6-philic domains and mesoporous transport channels for propylene/propane separation, Sep. Purif. Technol. 305 (2022) 122436, doi:10.1016/j.seppur.2022.122436.

[31] Z. Hu, Y. Wang, B.B. Shah, D. Zhao, CO_2 capture in metal-organic framework adsorbents: an engineering perspective, Adv. Sustain. Syst. 3 (2019) 1800080, doi:10.1002/adsu.201800080.

[32] S. Xu, W.C. Li, C.T. Wang, L. Tang, G.P. Hao, A.H. Lu, Self-pillared ultramicroporous carbon nanoplates for selective separation of CH_4/N_2, Angew. Chem. Int. Ed. 133 (12) (2021) 6409–6413, doi:10.1002/ange.20201423.

[33] J. Liu, Y. Liu, D.K. Talay, E. Calverley, M. Brayden, M. Martinez, A new carbon molecular sieve for propylene/propane separations, Carbon 85 (2015) 201–211, doi:10.1016/j.carbon.2014.12.089.

[34] K.A. Cychosz, R. Guillet-Nicolas, J. García-Martínez, M. Thommes, Recent advances in the textural characterization of hierarchically structured nanoporous materials, Chem. Soc. Rev. 46 (2) (2017) 389–414, doi:10.1039/c6cs00391e.

[35] L.S. Blankenship, J. Jagiello, R. Mokaya, Confirmation of pore formation mechanisms in biochars and activated carbons by dual isotherm analysis, Mater. Adv. 3 (9) (2022) 3961–3971, doi:10.1039/D2MA00141A.

[36] S. Du, J. Huang, A.W. Anjum, J. Xiao, Z. Li, A novel mechanism of controlling ultramicropore size in carbons at sub-angstrom level for molecular sieving of propylene/propane mixtures, J. Mater. Chem. A 9 (42) (2021) 23873–23881, doi:10.1039/d1ta07261g.

[37] Y. Dong, Q. Zhang, Z. Tian, B. Li, W. Yan, S. Wang, K. Jiang, J. Su, C.W. Oloman, E.L. Gyenge, R. Ge, Z. Lu, X. Ji, L. Chen, Ammonia thermal treatment toward topological defects in porous carbon for enhanced carbon dioxide electroreduction, Adv. Mater. 32 (2020) 2001300, doi:10.1002/adma.202001300.

[38] S.Y. Tang, Y.S. Wang, Y.F. Yuan, Y.Q. Ba, L.Q. Wang, G.P. Hao, A.H. Lu, Hydrophilic carbon monoliths derived from metal-organic frameworks@ resorcinol-formaldehyde resin for atmospheric water harvesting, New Carbon Mater. 37 (1) (2022) 237–244, doi:10.1016/S1872-5805(22)60576-6.

[39] S. Tanaka, K. Fujita, Y. Miyake, M. Miyamoto, Y. Hasegawa, T. Makino, S. Van der Perre, J.C.S. Remi, T. Van Assche, G.V. Baron, J.F.M. Denayer, Adsorption and diffusion phenomena in crystal size engineered ZIF-8 MOF, J. Phys. Chem. C 119 (51) (2015) 28430–28439, doi:10.1021/acs.jpcc.5b09520.